WATER RESOURCES RESEARCH, VOL. 33, NO. 6, PAGES 1287–1295, JUNE 1997

Water film flow along fracture surfaces of porous rock

Tetsu K. Tokunaga and Jiamin Wan
Lawrence Berkeley National Laboratory, Berkeley, California

Abstract. This study shows that hydraulic properties of individual fracture surfaces can be meaningfully defined and measured, and that water film flow is a mechanism contributing to fast, unsaturated flow in fractures. The hydraulic conductivity of an unconfined block of Bishop Tuff was measured over a range of near-zero matric potentials, where differences between hydraulic conductivities obtained without and with wax sealing of its lateral sides allowed isolation of film flow effects. Tensiometer and flux measurements showed that surface film flow in this system was significant for matric potentials greater (more positive) than about −250 Pa. In this range the average film thickness was shown to be potential dependent and proportional to the observed enhanced hydraulic conductivity. Measured average surface film thicknesses ranged from 2 to 70 μm, with average film velocities in the range of 2 to 40 m d^{-1} (about 10^3 times faster than that of the pore water under unit gradient saturated flow). Our experiments demonstrate that hydraulic properties of macroscopic surfaces of porous media are quantifiable, related to surface roughness, and potentially important in the flow of water in vadose environments. This study further shows that contrary to existing conceptual models, unsaturated flow in fractures cannot generally be predicted solely on the basis of aperture distribution information. The high velocities of these surface films suggest that film flow can be an important mechanism contributing to fast flow in unsaturated fractures and macropores, especially in media characterized by low-permeability matrix and along regions of convergent flow in partially saturated fractures.

Introduction

Flow of water through unsaturated soil and rock is an important segment of the hydrologic cycle, especially in arid and semiarid regions, as well as in areas with substantial depths to the water table [*Evans and Nicholson*, 1987; *Stephens*, 1994]. Preferential flow of infiltrating water through very small regions within partially saturated soils, via macropores, has been recognized as an important feature of water infiltration [*White*, 1985]. Trends in flow rates and chemistry of seeps within Rainier Mesa, Nevada [*Russell et al.*, 1988; *Wang et al.*, 1993], and the occurrence of bomb-pulse chlorine 36 in fractured or faulted zones of Yucca Mountain, Nevada [*Fabryka-Martin et al.*, 1996], have demonstrated that fast flow phenomena also occur in deep, partially saturated, fractured tuffs. Gaining an understanding of mechanisms responsible for such fast flow is important not only in the further development of vadose zone hydrology but also for many practical purposes relating to vadose zone contaminant transport and groundwater contamination. Whether or not preferential flow along fractures or macropores occurs depends strongly on matric potential, ψ, the water content-dependent component of the soil water chemical potential [*Hillel*, 1980; *Sposito*, 1981]. At low and high extremes of ψ, fractures are fully desaturated and fully saturated, respectively. The theory of flow through saturated fractures has undergone much development [*Zimmerman and Bodvarsson*, 1996]. In contrast, understanding of flow and transport in partially saturated fractures is still evolving, especially with respect to small-scale mechanisms and their impact on larger-scale processes [*Glass et al.*, 1995].

Paper number 97WR00473.
0043-1397/97WR-00473$09.00

Existing conceptual models of unsaturated flow within fractures depend fundamentally on aperture distributions [*Wang and Narasimhan*, 1985; *Pruess and Wang*, 1987; *Pruess and Tsang*, 1990; *Wang and Narasimhan*, 1993]. The ψ dependence of unsaturated fracture hydraulic properties has been conceptualized based on an inverse relation between local aperture size and magnitude of its water- and air-entry values of ψ. This conceptual application of the Laplace capillary pressure equation prevents water filling of the largest apertures until ψ comes close to zero (i.e., water pressure approaching local atmospheric pressure). The aperture-based model of water distribution in unsaturated fractures is illustrated in Figure 1a, which depicts a cross section through a variable-aperture fracture with water occurring at isolated locations corresponding to contact points or aperture minima. Flow and transport between adjacent matrix blocks and across the partially saturated fracture plane is permitted in this model through hydraulic connections at aperture minima. It is important to note that in the context of models based strictly on aperture distributions, microscale regions along the fracture plane are either fully saturated (hydraulically conductive) or fully desaturated (nonconductive). Therefore aperture-based conceptualizations predict that unsaturated flow along the fracture plane depends strongly on continuity of locally saturated (conductive) aperture segments. Mechanistic models of fast flow through unsaturated tuffs have considered episodic, high infiltration events which permit transient pulses of water to migrate downwards via saturated flow in fractures with simultaneous matrix imbibition of water [*Nitao and Buscheck*, 1991; *Wang et al.*, 1993].

Aperture-based predictions of strong phase interference in fracture relative permeabilities have been demonstrated in experiments conducted on epoxy fracture casts [*Persoff and Pruess*, 1995]. Epoxy casts are useful in visualization of unsat-

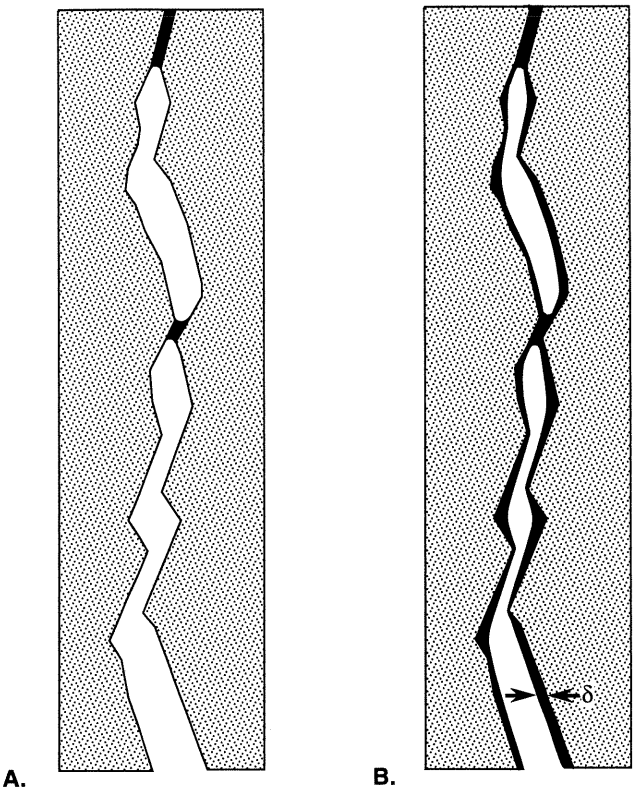

Figure 1. Two conceptual models of the distribution of water in fractures. (a) Aperture-based model. (b) Inclusion of surface films with aperture considerations. The film thickness at a specific location is denoted by δ.

urated fracture flow phenomena that could occur in nonporous rock. However, the incomplete water wettability of epoxy surfaces itself promotes phase interference by not allowing the spreading of water films and hence not allowing coexistence of water and air within a common segment of fracture. Incomplete surface wettability may prohibit extension of results obtained on epoxy casts to certain aspects of unsaturated fracture flow in fully wettable porous rock. To our knowledge, the aperture-based model has not been experimentally tested on fractured, porous rock. Furthermore, much of the previously mentioned evidence of fast flow in fractures as well as macropores lacks direct evidence of continuous, saturated pathways. These considerations leave open the possibility of additional mechanisms which control unsaturated flow in fractures.

Film flow of water along macropore or fracture surfaces could reconcile the paradoxical occurrence of fast flow in unsaturated channels [*Beven and Germann*, 1981; *Germann*, 1990]. Our alternative conceptual model of unsaturated flow in fractures allows water to exist in continuous films as well as in pendular regions associated with aperture minima. This alternative depiction of unsaturated flow in fractures is shown in Figure 1b. Note that in this alternative model, film continuity could allow for fast flow in unsaturated fractures, given sufficiently transmissive films. Also note that in cases where film flow is significant, the aperture-based model will be incapable of correctly predicting unsaturated flow in fractures. Thus, if the film flow phenomenon is significant in unsaturated flow in fractures, revision of earlier aperture-based models is indicated. However, at this time direct measurements of film thicknesses, film velocities, and their dependence on matric potential appear to be lacking in studies of flow in soil and rock.

Several observations lead us to consider film flow as a mechanism for fast flow through the vadose zone. The possible development of film thicknesses to the extent that gravity-driven flow would become hydraulically significant is suggestive from the very steep rise of water vapor adsorption isotherms as the activity of water approaches unity [e.g., *Orchiston*, 1953; *Kemper and Rollins*, 1966; *Taylor and Ashcroft*, 1972]. Episodic rainstorms over clayey soils with large, surface-exposed shrinkage cracks result in much of the infiltrating water running off upper low-permeability surfaces and flowing downwards along lateral surfaces of large soil aggregates [*Bouma and Dekker*, 1978]. This process also contributes to recycling of clays (i.e., colloid transport) in Vertisols [*Buol et al.*, 1973]. The aperture or pore-size distribution is of little significance in characterizing such flows when openings are large enough to sustain film flow along opposing surfaces of cracks, separated by an air gap. Recent experiments in glass micromodels suggested that hydraulic properties of rough surfaces can become important even when fracture apertures are still essentially unsaturated [*Wan et al.*, 1996]. The relatively negative ψ characteristic of average conditions in fractured tuff in arid and semiarid regions probably prevents the persistence of high fracture saturations in the vadose zone and probably minimizes the hydrologic importance of water films along many unsaturated fracture surfaces [*Taylor and Ashcroft*, 1972; *Evans*, 1983]. However, the previously mentioned chemical and isotopic evidence from these environments suggest that film flow might be important on fracture surfaces which occur along pathways of focused flow and during transient, high-infiltration events.

Here we present and test a conceptual model of gravity-driven water film flow at near-zero matric potentials, along macroscopic rock fracture surfaces. In this study, "near-zero" refers generally to the range of main wetting curve matric potentials over which the rock matrix is effectively water saturated [*Klute*, 1986]. In this range of matric potentials the water-air interface is able to expand outward from matrix pores into fracture surface roughness features as described in the next section. While the general case of unsaturated flow in fractures is expected to include contributions of water in films and in aperture minima (Fig. 1b), our present study is concerned with quantifying film flow. In order to isolate the film aspect, we focused this investigation on the "large aperture limit," in which case water could not accumulated in local aperture minima. This limit may be equated with the hydraulic behavior of single rock surfaces. In presenting the conceptual model we provide estimates of film thicknesses required to permit fast, gravity-driven flow and introduce the relevance of surface roughness on film flow. In our experimental testing, we isolated the ψ-dependent film transmissivity through differences in hydraulic conductivities measured on a tuff without and with sealing of its lateral surfaces. A method was also developed to measure the ψ dependence of average film thicknesses on fracture surfaces. Combining these types of measurements permits calculation of average film velocities along rough fracture surfaces and comparison with the smooth film case.

Conceptual Model

The conceptual model proposed here is that of ψ-dependent thicknesses of conductive water films along macroscopic sur-

faces of rock and soil. This concept might be applicable to a wide range of natural surfaces. These include flows along individual sides of fracture pathways through rock, surfaces of soil aggregates, seepage faces, and surfaces of caves and excavations [*Philip et al.*, 1989]. The wetting characteristics of a natural rough surface have previously been approximated by simple corrugated surfaces [*Philip*, 1978]. Other models have also been developed for flows along or transverse to concaved surface features [*Pozrikidis*, 1988; *Ransohoff and Radke*, 1988; *Zhao and Cerro*, 1992; *Shetty and Cerro*, 1993; *Dong and Chatzis*, 1995; *Rye et al.*, 1996]. The models concerned with uniformly corrugated surfaces generally provide expressions for the film thickness, δ, and dependence on ψ and predict that thickness increases to magnitudes similar to that of the surface roughness as the ψ approaches zero. From the theoretical work on simple surfaces it becomes clear that the topography of surfaces of rock and soil aggregates control surface hydraulic properties. Since most natural rock and soil aggregate surfaces are complex, the quantitative usefulness of models based on simple geometries may be poor, especially with respect to predicting flow. Nevertheless, the importance of the characteristic amplitudes of surface depressions, R, prevails in the near-zero matric potential limit because δ becomes similar to this dimension. From the Laplace capillary equation the matric potential at which films begin to significantly rise above local surface minima (when depths and widths are of similar dimensions) will be on the order of $-\gamma/R$, where γ is the surface tension of the water-air interface. Local minima with depths of 0.1 and 1 mm will begin significant filling at ψ of about -700 and -70 Pa, respectively. Since real fracture surfaces are composed of a wide spectrum of roughnesses, with finer-scale features embedded within coarser ones, it is expected that average film thickness will often increase continuously with ψ.

The combined effects of adsorbed film thickening and increasing water-air interfacial radii of curvature as ψ approaches zero leads to an overall thickening of surface films. A complete analysis $\delta(\psi)$ for a corrugated surface, including calculations of effects of both capillarity and adsorption, is provided by *Philip* [1978]. In the near-zero matric potential limit, where water films build up in thickness comparable to local surface roughness, it is reasonable to expect that their contribution to water flow can become important. This would be especially true when the bulk soil or rock is characterized by low permeability. The simplest model for unit-gradient, downwards flow of a water film assumes a film of uniform thickness δ, flowing down a smooth surface [*Bird et al.*, 1960]. The velocity profile is parabolic, and the average velocity is given by

$$\bar{v} = \frac{\rho g}{3\eta}\,\delta^2, \tag{1}$$

where g is the acceleration due to gravity, and ρ and η are the density and dynamic viscosity of water, respectively. The unique geometries of real rock and soil aggregate surfaces result in considerably more complex surface velocity profiles than any of these simpler models. Additional complications associated with natural systems include nonuniform boundary conditions, variations in macroscopic surface inclination, and variations in surface wettability. Despite all of these factors, the mobility of unconfined films under the influence of gravity can be expected to be at least locally significant at near-zero matric potentials. Equation (1) shows that a 10-μm-thick (uniformly so) falling film (at 25°C) will have an average velocity of 28 m d^{-1}. While surfaces of natural rock and soil aggregates seldom are smooth or precisely vertically oriented, the above calculation may provide an estimate of the significance of falling film flow. This estimate suggests that films of similar thickness can be effective in rapidly transporting water and solutes downwards through the vadose zone. The potential hydrologic significance of falling film flow may be greatest along rougher surfaces of lower permeability media since film thicknesses can become greater, since pore water velocities in the bulk medium will be relatively low, and since the "near-zero" ψ condition encompasses a broader range.

Materials and Methods

A fragment of Bishop Tuff (see work by *Hildreth* [1979] for rock description), broken off of an exposed fractured block (Chidago Canyon, Mono County, California) provided both samples for this investigation. These samples of the ash-fall tuff have porosities of 0.33, with no apparent microfracture features. On the first test sample, horizontal top and bottom surfaces were cut, leaving a final block height of 52 mm (Figure 2). The slightly varying cross-sectional area (in the horizontal) was $2.8 \times 10^3 \pm 0.2 \times 10^3$ mm^2. The lateral surfaces were left in original rough form (fracture surfaces), except for one edge strip, which was vertically cut and polished for later comparison of surface flow features. Although cutting and polishing probably contributed to some clogging of pores, all experiments were conducted after extensive water permeation (about 20 pore volumes), which ensured stable hydraulic behavior. Pairs of horizontal, 2-mm-diameter holes were drilled at 10-mm vertical separations relative to the upper and lower block surfaces and connected to variable reluctance pressure transducers (Validyne model DP15-22, range 1400 Pa, Validyne Engineering Corp., Northridge, California) via 1.6-mm-I.D., water-filled tubing (epoxy sealed at the rock-tube contact). Variable reluctance pressure transducers are well suited for measuring small differential pressures [*Fraden*, 1993]. The tensiometer holes were drilled completely through the rock, permitting effective purging of any accumulated air bubbles. The pressure transducers, tubing, and pressure ports within the block were operated as tensiometers [*Cassel and Klute*, 1986], providing direct measurements of local hydraulic potential. It was not necessary to use a ceramic interface between the water-filled tubing and rock because experiments were conducted at ψ very close to zero, and within the effective air-entry limit of the tuff (≈ -500 Pa). Additional tensiometer measurements were made directly on the sidewalls of the tuff, using a "surface tensiometer" [*Tokunaga*, this issue]. This device permits direct measurement of ψ on bulk surfaces of porous media. Such measurements are made by placing the surface tensiometer's sensing tip directly on the rock surface. All pressure transducer readings were accurate to ± 3 Pa, with calibrations performed by varying the vertical distance between transducers and a free water surface. Vertical distances were measured with a cathetometer with a resolution of 0.1 mm (Eberbach Corp., Ann Arbor, Michigan). Experiments were carried out above the effective air-entry ψ values of the tensiometer-rock system, as verified by hydrostatic tests and occasional purging of water-filled tubes to check for air-bubble accumulation. The test block was placed on the top surface of a large, coarse grade fritted glass filter funnel, with an intervening sheet of glass fiber filter (Gelman type A/E) to provide better hydraulic continuity (Figure 3). The lower boundary was regulated at selected hydraulic potentials via adjustment of the water level in

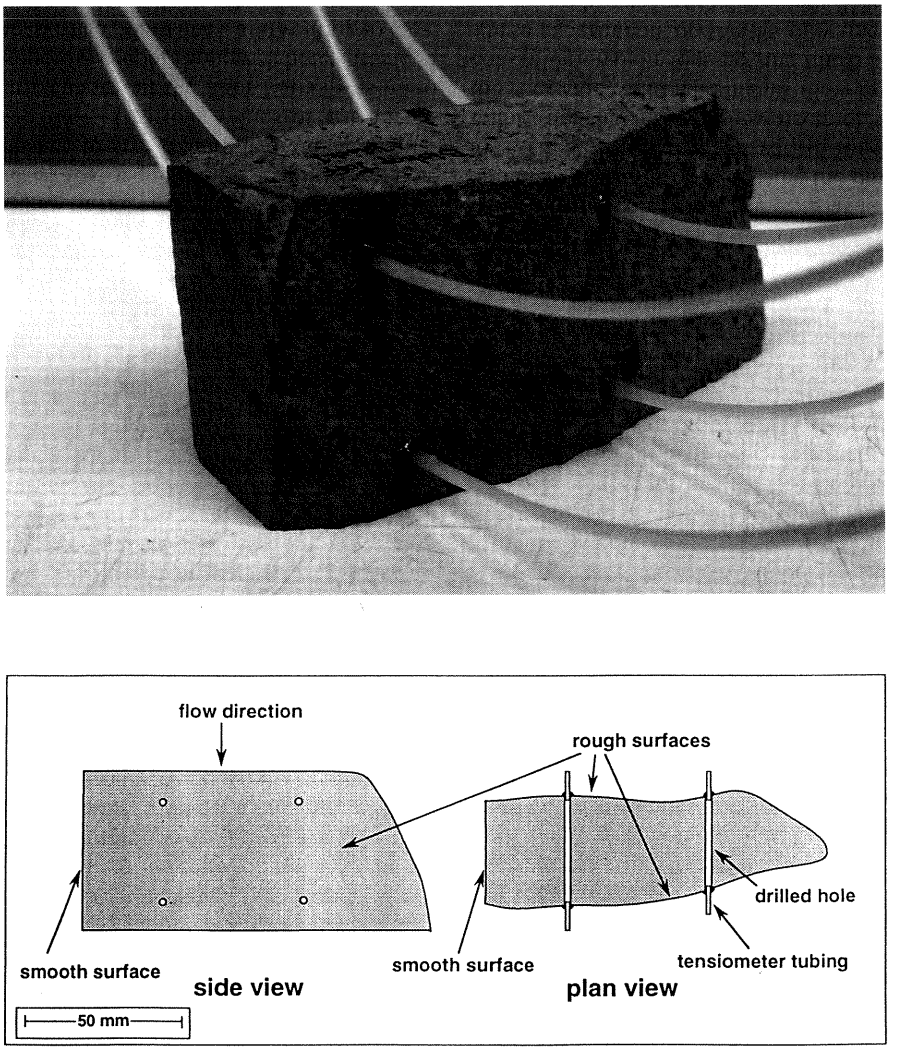

Figure 2. Block sample of Bishop Tuff for K versus ψ measurements (unsealed). Note the single vertically cut and polished edge on the left side. Also shown are the tensiometer lines.

an outflow reservoir. An additional sheet of glass fiber filter was placed along the top surface of the rock block to facilitate distribution of water supplied to the top of the block via a pair of syringe pumps (model 55-4140, Harvard Apparatus, Inc., South Natick, Massachusetts). The rock was first wetted by imbibition from the bottom boundary, followed by continuous permeation of water from the upper surface. As noted previously, about 20 pore volumes of water were permeated through the sample prior to initiation of experiments. Purging was conducted at $\psi \approx -400$ Pa.

The first series of experiments was performed to determine the hydraulic conductivity of the rock, including possible film flow contributions, $K(\psi)$. A sequence of steady state flow conditions were established to provide unit hydraulic potential gradient, gravity-driven flow at various values of ψ (ranging from -470 to -10 Pa). The top of the filter funnel was fitted with an acrylic lid to suppress evaporation, with holes provided for tensiometer tubing, syringe pump lines, and venting to local atmospheric pressure. The relative humidity in the test chamber (interior of the covered filter funnel) was maintained at nearly 100%. This high value results from the surface of the fritted glass filter acting not only as a regulator of the matric potential at the bottom of the rock block but also as a regulator of the water potential (relative humidity) in the chamber. Unit hydraulic potential gradient conditions were established by adjusting both the upper supply flow rate and bottom boundary hydraulic potential such that all tensiometers indicated a common value of ψ (typically to within ± 10 Pa, and in worst cases to within ± 15 Pa). Gradients larger than unity were diminished by either raising the lower boundary reservoir or adjusting the syringe pump speed to a lower rate, or a combination of both. The magnitude of the gradient indicated the magnitude of the necessary adjustments. Gradients lower than unity were corrected in the converse manner, that is, through lowering the boundary reservoir or increasing the pump speed or both. The lowest flow rate coincided with a range of ψ over which no visible flowing films (light-reflecting) were observable along the rock side walls. The highest flow rate provided unit gradient conditions, obvious flowing films, and $\psi = -10 \pm 10$ Pa. These experiments on the laterally unconfined block were repeated on two different days, with flow rates and ψ monotonically increased and then decreased. Typical times to steady state following a step change in boundary conditions were about 20 min.

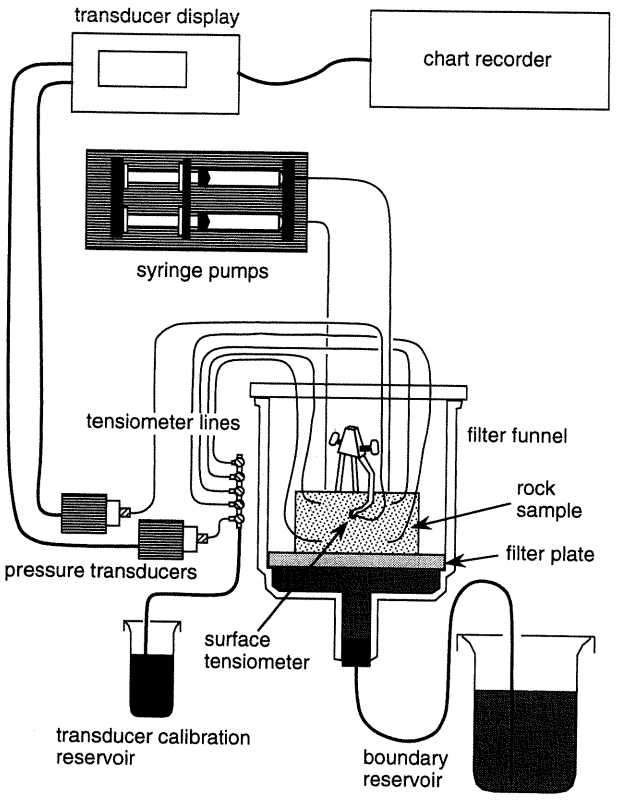

Figure 3. Apparatus for K versus ψ measurements.

Following these determinations of $K(\psi)$ for the rock (bulk and possible surface contributions), qualitative tests for flow along the lateral surfaces was performed. This involved supplying a water-soluble blue dye tracer at rates previously indicative of providing significant surface film flow and photographically recording the descent of the dye front.

A final set of measurements was made to determine the block's hydraulic conductivity in the absence of surface flow effects. For these last permeability measurements, the block was air dried, its lateral surfaces were wax sealed, and it was returned to the test chamber for rewetting in the manner described previously. As before, a series of unit-gradient flow conditions were established and recorded. Differences between measurements at a given ψ, before and after sealing of sidewalls, were attributed to surface film flow. Gravimetric water contents were determined on the unsealed and sealed rock following each experiment in order to determine whether or not entrapped air contributed to observed differences in hydraulic responses.

In order to facilitate interpretation of surface flow, some measure of δ, and $\delta(\psi)$, was needed. Measurements of average surface film thickness, $\bar{\delta}$, were obtained via modification of the conventional tension plate method for determining moisture characteristics [*Hillel*, 1980; *Klute*, 1986]. For this determination a second test sample, consisting of a 40-mm by 60-mm by about 12-mm-thick slab, was cut from the original rock (adjacent to the permeability test sample). The side and bottom surfaces were polished flat and sealed. The surface oriented upwards was left in its original rough condition. This surface had a maximum variation in "elevation" of 3 mm, with more than 95% of the area restricted to a 2 mm variation. Finer, grain-scale surface roughness ranged from about 50 to 500 μm (visual observation). These surface features (fine and coarse scale) were very similar to those of the unsealed sidewalls of the permeability test block. Three parallel horizontal holes were drilled from one side, 80% through the block, and connected to a water reservoir via water-filled tubing (Figure 4). The rock slab was placed, fracture surface oriented upwards, in a sealable chamber (to prevent evaporation) which was pinhole vented to maintain exposure to local atmospheric pressure. The water reservoir was placed on an analytical balance in a sealed, humidified chamber. Humidification of the balance chamber prevented drift of the balance due to small evaporative losses. After the block was presaturated, the water content dependence on ψ was determined over a narrow range by raising and lowering the block chamber relative to the free water surface and recording the mass of water exchanged. Matric potential values were varied from -420 to -15 Pa, ± 15 Pa, along the rough surface. The range of ± 15 Pa within any given equilibration is due to the fact that the rough surface elevation ranges ± 1.5 mm relative to the mean value. Water exchange during this experiment represented the combined effects of slight changes in saturation of the bulk block and changes in water film thickness along the unsealed rough sur-

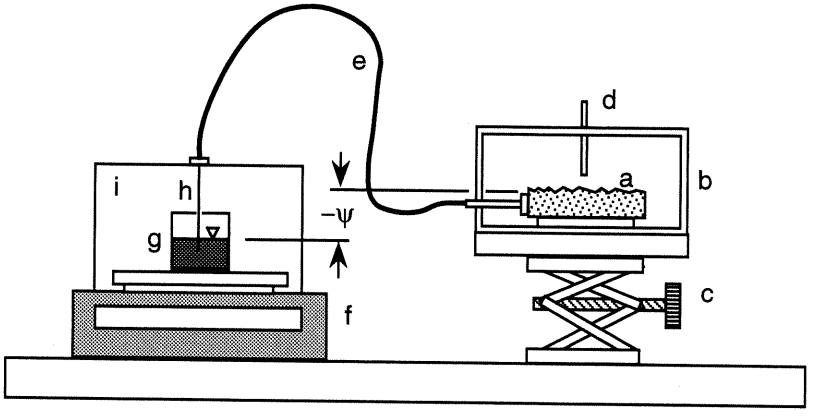

Figure 4. Apparatus for determining bulk matrix saturation and average film thickness versus ψ. The components shown are (a) rock sample, (b) sealed chamber (pin-hole vented), (c) laboratory jack stand, (d) thermometer, (e) water-filled tubing, (f) electronic balance, (g) water reservoir, (h) hypodermic needle, and (i) evaporation barrier.

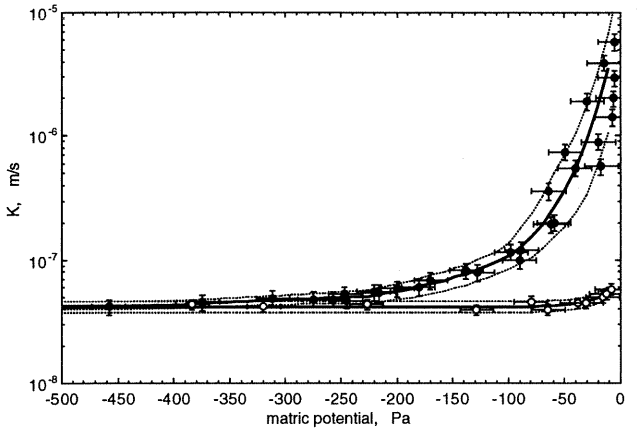

Figure 5. Results of $K(\psi)$ measurements on the unsealed (solid circles) and laterally sealed (open circles) tuff block. The surface flow component $K(\psi)$ of was taken as the difference between the two fitted curves and used to calculate both $T(\psi)$ and $\bar{v}$. Error bars associated with individual points indicate maximum uncertainties in ψ of ± 15 Pa, and maximum uncertainties in $K(\psi)$ of up to $\pm 15\%$, as discussed in the text. Also shown are uncertainty envelope curves, which grow from $\pm 10\%$ at low ψ up to $\pm 80\%$ at high ψ in the unsealed tuff and remain at $\pm 10\%$ for the laterally sealed measurements.

face. Following two wetting-draining cycles in which water retention on natural rough fracture surfaces was measured, the block was removed from the apparatus and dried. To prepare for similar tests on a smoothed surface of Bishop Tuff, the rough surface was ground and polished flat (final roughness ~ 50 μm), parallel to the base of the block, resulting in a loss of 15% of the original rough slab mass. The smoothed slab was resaturated with water, and reconnected to the apparatus. A final set of draining-wetting cycles was performed over the ψ range of -400 to -5, ± 5 Pa, at the upper surface of the block. In this case the range of ± 5 Pa is due to smooth surface elevation uncertainties associated with slight tilting of the block upon raising and lowering the platform (± 0.5 mm). Mass exchanges during this stage were associated with the bulk block and its smooth upper surface. These mass exchange values were increased by 18% in order to be normalized to the original rough block mass. In other words, mass exchanges on the smoothed block (which had 85% of the original rough block pore volume) were scaled up by a factor of 1.18 to compensate for the matrix pore volume removed by smoothing ($1.18 \times 0.85 = 1.00$). The differences between results on the original rough versus (normalized) smooth surface were attributed to water film storage along the rough surface.

Results and Discussion

The hydraulic conductivity of the unsealed block increases steeply as the matric potential approaches zero, whereas relatively little change was measured in the sealed case (Figure 5). For the sealed system the conventional definition of hydraulic conductivity remains useful, and measured permeabilities ranged from $k = 4 \times 10^{-15}$ m^2 to 6×10^{-15} m^2. Artifacts due to entrapped air are considered insignificant in explaining differences between these two curves because essentially identical gravimetric water contents were measured in both cases (0.206 and 0.208, for the unsealed and sealed rock, respectively). Maximum likely uncertainties in individual values of $K(\psi)$ shown in Figure 5 are due primarily to the composite uncertainties in ψ (deviations from uniform ψ within the sample under ideal unit gradient flow) and ranges in pump rates which yielded essentially identical ψ under unit gradient conditions. Also shown in Figure 5 are uncertainty envelope curves for the $K(\psi)$ relations, used later to estimate composite uncertainties of derived values (transmissivities and film velocities). Broadening of the uncertainty limits in the very near zero ψ range ($\psi > -100$ Pa) for the unsealed runs might have been due to perturbations in thicker films. The comparison of $K(\psi)$ for the sealed versus unsealed block, along with the development of visibly observable flowing water films on all lateral surfaces for $\psi > -200$ Pa (matric head > -20 mm), indicates that enhanced conduction of water was due to film flow. The stable, unit-gradient flows, with measured values of $\psi < 0$, indicated that water in the flowing films was still below local atmospheric pressure. The "subatmospheric" state of water in these flowing films was further supported by tensiometer measurements made directly on the rock surface [*Tokunaga*, this issue]. These surface ψ readings were within ± 10 Pa of the bulk rock tensiometer values. In both the unsealed and sealed systems the hydraulic conductivity is defined here as the unit-gradient volumetric flux of water divided by the cross-sectional area of the block. In other words, the contribution of film thickness along the exposed lateral surfaces of the rock is taken as an insignificant addition to the total cross-sectional area available to flow. Based on measured average film thicknesses (described later), the maximum ratio of film/block cross-sectional areas is about 7×10^{-3}. It is noted that for media with homogeneous hydraulic properties, K for the matrix is scale invariant, while this is not the case for area-normalized fluxes in systems permitting film flow along external surfaces. In the latter case, scale dependence of the film/block cross-sectional area will give rise to a scale-dependent $K(\psi)$ of the matrix plus films. Thus unique characterization is obtained through normalizing unit gradient volumetric film fluxes to the macroscopic length of fracture surface (transverse to flow). This ψ-dependent quantity will be defined here as the film transmissivity, $T(\psi)$, following representations of flow in fractures.

Calculations of $T(\psi)$ were done as an intermediate step in obtaining average film velocities. The volumetric film flux per unit length (transverse to flow) along the rock surface was calculated by taking the difference in $K(\psi)$ between unsealed and sealed cases (differences between interpolation curves in Figure 5) and multiplying this quantity by the rock area/perimeter ratio. Results show $T(\psi)$ to monotonically increase with ψ (Figure 6). Standard methods [*Taylor*, 1982] were used for estimating composite uncertainty envelopes of transmissivities (Figure 6) as well as of average film velocities, presented later. It is noted that for ψ more negative than about -200 Pa, the uncertainty envelopes of the two $K(\psi)$ relations overlap (Figure 5). Thus for $\psi < -200$ Pa the behavior of $T(\psi)$ is not well constrained in the present study because of poor resolution of small differences in unsealed versus sealed fluxes. However, $T(\psi)$ theoretically approaches the product of K times the average film thickness (both ψ dependent) as ψ decreases.

Moisture characteristics measured on the bulk rock (without rough surfaces) showed that the matrix was maintained at saturations greater than 98% (and usually >99%) for all situations investigated here, supporting our conclusion that enhanced flow effects were primarily surface associated. The water content dependence on ψ was reproducible between duplicate runs on the rough surface block and between dupli-

cate runs on the polished surface block, with closure errors within wetting-draining cycles less of than 5% (of mass exchanged over the cycle). Through comparing total water uptake values from the rough versus polished slab, it was determined that most (82%) of the water exchanged in this near-zero ψ range is associated with the rough surface of the test rock.

The average film thickness, $\bar{\delta}$, was calculated by taking the difference between the rough- and smooth-surface block data (the latter data were scaled up by a factor of 1.18 to account for the 15% matrix mass lost due to smoothing) and dividing by the macroscopic surface area (Figure 7). In this calculation the uncertainty in mass differences was about 3 mg per 100 Pa step change in ψ; $\bar{\delta}$ was not measurably significant on our apparatus until $\psi > -200$ Pa. This corresponds to the range of ψ at which K for the unsealed case begins to increase significantly, and the rock surface becomes reflective to visible light; $\bar{\delta}$ increases approximately exponentially as ψ approaches zero. It should be noted that the distribution of film thicknesses also increases with increased (closer to zero) ψ. This was qualitatively observed and is due to contributions from both very thick films (water-filled local surface depressions) and thin films (bridging over local ridges). The latter regions can contribute significantly to resistance in surface flows. Previous studies on wetting film statics and dynamics also illustrate this phenomenon of broadening film thickness distributions in the limit of ψ approaching zero [e.g., *Philip*, 1978; *Shetty and Cerro*, 1993].

It is also worth noting that wetting-draining moisture characteristics of hydrophilic porous media surfaces, unlike bulk porous media, are expected to be nonhysteretic. None of the commonly recognized mechanisms [e.g., *Hillel*, 1980] responsible for hysteresis in moisture characteristics of nondeforming bulk porous media, the "ink-bottle" effect, contact angle hysteresis, and gas phase entrapment, apply in the present case. Each local depression can fill and drain via exchanges with the water-saturated interior rather than solely through the surface network of depressions. As long as no reversals in "effective pore size" are encountered within individual surface depressions during continuous advances (wetting) or retreats (draining) of menisci, no ink-bottle-type hysteresis in the surface moisture characteristic relation should arise. Hysteresis due to contact angle variations is also not expected in this system since

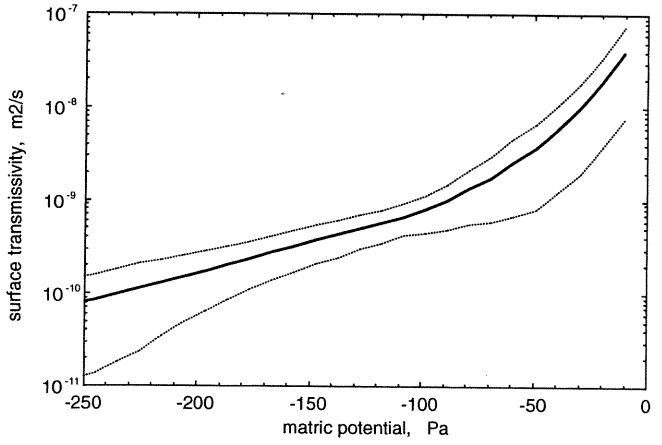

Figure 6. Surface film $T(\psi)$ shown in the solid line, based on differences between unsealed and sealed block $K(\psi)$. The dotted lines indicate the uncertainty envelopes.

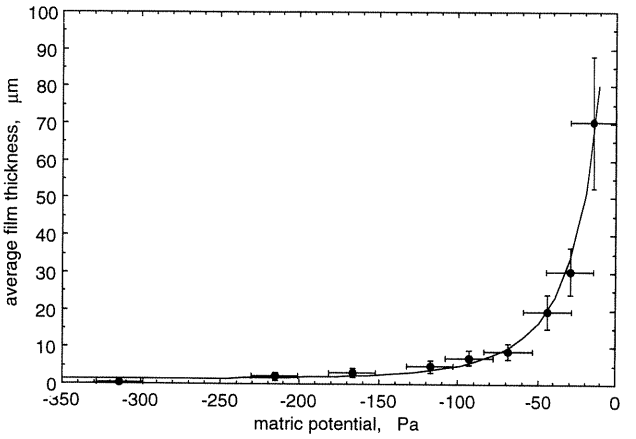

Figure 7. Average thicknesses of surface films versus ψ. Data points are averages of duplicate measurements. The range of ± 15 Pa within any given equilibration is due to the fact that the rough surface elevation ranges ± 1.5 mm relative to the mean value. The minimum uncertainty in mass differences was about 3 mg per 100 Pa step change in ψ, equivalent to a minimum uncertainty in thickness of about ± 1 μm. Wider range bars span twice the thickness range of duplicate measurements.

all rock surfaces are already wet. Finally, hysteresis due to gas phase entrapment is not possible since the surface film gas-water interfaces is always in direct contact with a bulk gas phase. Insufficient data were collected along redraining cycles of the current study to quantitatively test for hysteresis in the surface moisture characteristic. It will be examined in detail in future work. The extent to which this work can be transferable to essentially impermeable hard rock is not currently understood. Anticipated complications include the strong influence of surface wettability, and reintroduction of hysteresis in $S(\psi)$ and $T(\psi)$. Hysteresis would arise in this case from the dependence of δ within individual surface depressions on exchanges of water solely through surface films connected to neighboring depressions and from contact angle variations. In such situations, the surface would behave much more like a two-dimensional pore network. Aside from the contact angle effects, hysteresis arises from variable pore-size and variable depression-depth, in wetting of porous media and rough solid surfaces, respectively.

Two approaches were taken to calculating average surface film velocities, $\bar{v}$. In the first approach $T(\psi)$ was divided by $\bar{\delta}$. This approach is based solely on direct measurements and is therefore considered reliable. In the second approach, $\bar{\delta}$ was simply substituted into the smooth film formula, assuming (1) could provide estimates of $\bar{v}$ on more complex surfaces. Results from the two approaches (Figure 8) differ with respect to specific trends, although they remain within an order of magnitude of each other over most of the quantifiable range. The smooth film model predicts a much larger variation of $\bar{v}$ with ψ, indicative of the δ^2 dependence of this model. Smooth film calculations progressively overestimated the actual film flow contributions over the higher ψ range (-50 to -15 Pa). At the highest potential the smooth film approximation overestimated average film flow by about 50-fold. The smooth film approximation includes neither the effects of surface tortuosity nor local minima in film thicknesses along flow paths. The latter factor is believed to be especially important in the near-zero ψ limit since the distribution of film thicknesses is greatest in this

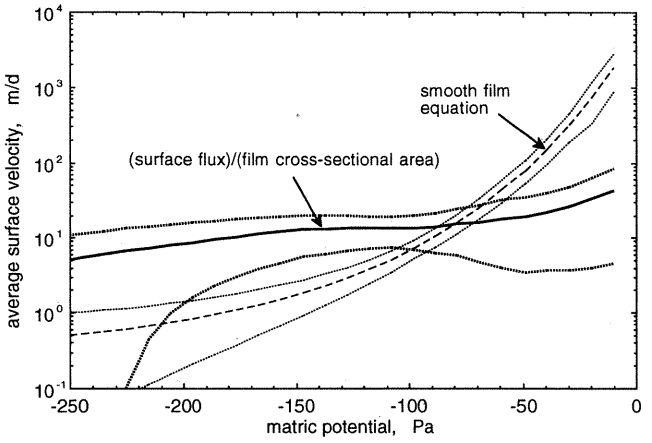

Figure 8. Calculated average film velocities, based upon dividing $T(\psi)$ by $\bar{\delta}$ and on equivalent smooth film calculations. The dotted lines indicate the uncertainty envelopes.

limit and since $\bar{\delta}$ values cannot account for the higher resistance encountered as water is forced to flow through locally thin zones. Directly calculated average film velocities based on $T/\bar{\delta}$, equivalent to dividing the surface-associated enhanced flux by the film cross-sectional area, exhibit broadening uncertainties at very near zero ψ and at $\psi < -200$ Pa. Uncertainty envelopes broaden for $\psi > -80$ Pa because of associated wider uncertainties in T and $\bar{\delta}$. Despite the greater uncertainties in this range of very near zero ψ, values of $\bar{v}$ are still constrained within ranges associated with fast flow. Uncertainty envelopes also broaden for $\psi < -200$ Pa, primarily because of poorly resolved differences in unsealed versus sealed $K(\psi)$. Note that despite uncertainties, best estimates of average film velocities obtained from $T/\bar{\delta}$ vary over the fairly narrow range of 5 to 60 m d^{-1}. A possible interpretation of the mild change in average velocity is that even as average film thicknesses build up with increased ψ, flow rates are largely controlled by locally thin film zones which maintain relatively constant hydraulic resistance. In this interpretation the increased surface flux with increased ψ then appears to result primarily from increased numbers of effectively conducting surface pathways. These calculated surface $\bar{v}$ are about 400 to 3000 times greater than the unit-gradient pore water velocity in this moderately permeable tuff, showing that surface film flow can be very significant in downwards transport of water and solutes.

Observations of the descent of the dye tracer down the rock surfaces provided qualitative evidence for the effectiveness of gravity-driven film flow. Tracer velocities were not quantitatively determined, but the visible advances down the rough surfaces were in the range of 0.5 to 10 m d^{-1}, with apparent fingering within continuous, deeper channels. Use of the dye tracer also permitted a qualitative test of the influence of surface roughness on film flow. In one run with dye injection, the source was placed on the upper rock surface, very near the single vertically cut and polished end (Figure 2) in order to compare flow down smooth versus rough surfaces. Despite the fact that the source was placed about three times closer to the smooth vertical segment, the tracer was observed to preferentially flow only down the nearest accessible rough sides, indicating that the latter pathway offered much less resistance. This behavior provides further evidence for the important role of surface roughness in gravity-driven flows at near-zero ψ.

Conclusions

In this study we proposed that film flow can be an important mechanism behind unsaturated flow in fractures. We introduced concepts of fracture surface transmissivities and fracture surface moisture characteristics and experimentally demonstrated that hydraulic properties can be meaningfully assigned to macroscopic surfaces of porous rock. The concepts developed here, of ψ-dependent surface transmissivities and surface moisture characteristics of consolidated rock (tuff), are probably transferable to surfaces of large soil aggregates. Our present results show that surface hydraulic properties become important at near-zero ψ, for a moderate-permeability tuff. Other cases are also worth considering. Surface hydraulic properties may be more significant in systems characterized by low permeabilities since (1) surface velocities will be higher than matrix pore water velocities over a wider range of ψ, and (2) lower sorptivities associated with low-permeability media sustain higher ψ along wetted external surfaces during transient infiltration events and permit deeper migration of water down fractures [*Wang et al.*, 1993]. Also recall that the "near-zero" ψ range was defined as the interval over which the local matrix is effectively at saturation, and that significant film flow is expected to be constrained within this range. Since the "near-zero" ψ range covers a wider energy interval in media with finer characteristic pore size, it is expected that film flow will also occur over wider ψ ranges in low permeability rock. At the opposite extreme, the possible importance of thin films at low ψ has been included in fractal analyses of matrix unsaturated hydraulic conductivities of porous media by *Toledo et al.* [1990].

Omission of surface film flow from general conceptual models of unsaturated flow in fractured porous media can lead to incorrect conclusions concerning flow and transport. The omission of film flow in aperture-based models results in underprediction of unsaturated fracture transmissivity relations. The commonly accepted notion that unsaturated, large-aperture fractures are nonconducting is clearly an oversimplification. This work demonstrates the capacity of natural, rough surfaces to conduct water at high velocities and under tension. Surface film flow may help explain observations of short travel times for solutes recovered from deep, unsaturated fractured rock [*Russell et al.*, 1988; *Nativ et al.*, 1995; *Fabryka-Martin et al.*, 1996]. Since conduction can take place through an interconnected network of local surface minima and within films which may be thin relative to aperture dimensions, water saturation–based approaches to detecting unsaturated fast flow pathways are not generally expected to succeed. While the present work indicates that energy-based approaches (i.e., tensiometry) can be sensitive indicators of surface flow, practical means for obtaining spatially comprehensive enough measurements to characterize field-scale preferential flow are lacking.

Despite the shortcomings of aperture-based models of unsaturated preferential flow, it would be equally erroneous to suggest that only surface hydraulic properties of fractures and macropores need to be determined. Mechanistically accurate models for unsaturated flow in fractures and macropores will require the combination of both aperture and surface contributions, with the complication that their effects will not generally be additive. The aforementioned postulate will be tested as part of the next stage of this study.

Acknowledgments. This work was carried out under U.S. Department of Energy contract DE-AC03-76SF00098. Additional support for

film thickness studies was provided by the U.S. Department of Energy, Basic Energy Sciences, Geosciences Research Program. We thank Robert W. Zimmerman and Sally M. Benson of Lawrence Berkeley National Laboratory for helpful comments on the draft manuscript and Todd C. Rasmussen (The University of Georgia), Scott Tyler (University of Nevada, Reno), and anonymous reviewers for additional useful suggestions.

References

Beven, K., and P. F. Germann, Water flow in soil macropores, II, A combined flow model, *J. Soil Sci., 32*, 15–29, 1981.

Bird, R. B., W. E. Stewart, and E. N. Lightfoot, *Transport Phenomena*, pp. 37–41, John Wiley, New York, 1960.

Bouma, J., and L. W. Dekker, A case study on infiltration into dry clay soil, I, Morphological observations, *Geoderma, 20*, 27–40, 1978.

Buol, S. W., F. D. Hole, and R. J. McCracken, *Soil Genesis and Classification*, Iowa State Univ. Press, Ames, 1973.

Cassel, D. K., and A. Klute, Water potential: Tensiometry, in *Methods of Soil Analysis, Part 1, Physical and Mineralogical Methods, Agron. Monogr. 9*, 2nd ed., pp. 563–596, Am. Soc. of Agron., Madison, Wis., 1986.

Dong, M., and I. Chatzis, The imbibition and flow of a wetting liquid along the corners of a square capillary tube, *J. Colloid Interface Sci., 172*, 278–288, 1995.

Evans, D. D., Unsaturated flow and transport through fractured rock-related to high-level waste repositories, final report, phase 1, *NUREG/CR-3206*, U.S. Nucl. Regul. Comm., Washington, D. C., 1983.

Evans, D. D., and T. J. Nicholson, Flow and transport through unsaturated rock: An overview, in *Flow and Transport Through Unsaturated Fractured Rock, Geophys. Monogr. Ser.*, vol. 42, D. D. Evans and T. J. Nicholson, pp. 1–10, AGU, Washington, D. C., 1987.

Fabryka-Martin, J. T., P. R. Dixon, S. Levy, B. Liu, H. J. Turin, and A. V. Wolfsberg, Summary report on chlorine-36 studies: Systematic sampling for chlorine-36 in the exploratory studies facility, *Level 4 Milestone Rep. 3783AD*, Los Alamos Natl. Lab., Los Alamos, N. M., 1996.

Fraden, J., *AIP Handbook of Modern Sensors, Physics, Designs and Applications*, 522 pp., Am. Inst. of Phys., New York, 1993.

Germann, P. F., Preferential flow and the generation of runoff, 1, Boundary layer flow theory, *Water Resour. Res., 26*, 3055–3063, 1990.

Glass, R. J., M. J. Nicholl, and V. C. Tidwell, Challenging models for flow in unsaturated, fractured rock through exploration of small scale processes, *Geophys. Res. Lett., 22*, 1457–1460, 1995.

Hildreth, W., The Bishop Tuff: Evidence for the origin of compositional zonation in silicic magma chambers, *Geol. Soc. Am. Spec. Pap. 180*, 43–75, 1979.

Hillel, D., *Fundamentals of Soil Physics*, 413 pp., Academic, San Diego, Calif., 1980.

Kemper, W. D., and J. B. Rollins, Osmotic efficiency coefficients across compacted clays, *Soil Sci. Soc. Am. Proc., 30*, 529–534, 1966.

Klute, A., Water retention: Laboratory methods, in *Methods of Soil Analysis, Part 1, Physical and Mineralogical Methods, Agron. Monogr. 9*, 2nd ed., pp. 635–662, Am. Soc. of Agron., Madison, Wis., 1986.

Nativ, R., E. Adar, O. Dahan, and M. Geyh, Water recharge and solute transport through the vadose zone of fractured chalk under desert conditions, *Water Resour. Res., 31*, 253–261, 1995.

Nitao, J., and T. Buscheck, Infiltration of a liquid front in an unsaturated, fractured porous medium, *Water Resour. Res., 27*, 2099–2112, 1991.

Orchiston, H. D., Adsorption of water vapor, I, Soils at 25°C, *Soil Sci., 76*, 453–665, 1953.

Persoff, P., and K. Pruess, Two-phase flow visualization and relative permeability measurement in natural rough-walled rock fractures, *Water Resour. Res., 31*, 1175–1186, 1995.

Philip, J. R., Adsorption and capillary condensation on rough surfaces, *J. Phys. Chem., 82*, 1379–1385, 1978.

Philip, J. R., J. H. Knight, and R. T. Waechter, Unsaturated seepage and subterranean holes: Conspectus, and exclusion problem for circular cylindrical cavities, *Water Resour. Res., 25*, 16–28, 1989.

Pozrikidis, C., The flow of a liquid film along a periodic wall, *J. Fluid Mech., 188*, 275–300, 1988.

Pruess, K., and Y. W. Tsang, On two-phase relative permeability and capillary pressure of rough-walled rock fractures, *Water Resour. Res., 26*, 1915–1926, 1990.

Pruess, K., and J. S. Y. Wang, Numerical modeling of isothermal and nonisothermal flow in unsaturated fractured rock: A review, in *Flow and Transport Through Unsaturated Fractured Rock, Geophys. Monogr. Ser.*, vol. 42, edited by D. D. Evans and T. J. Nicholson, pp. 11–21, AGU, Washington, D. C., 1987.

Ransohoff, T. C., and C. J. Radke, Laminar flow of a wetting liquid along corners of a predominantly gas-occupied noncircular pore, *J. Colloid Interface Sci., 121*, 392–401, 1988.

Russell, C. E., J. W. Hess, and S. W. Tyler, Hydrogeological investigations of flow in fractured tuffs, Rainier Mesa, Nevada Test Site, *DOE/NV/10384-21*, Desert Res. Inst., Las Vegas, Nev., 1988.

Rye, R. R., J. A. Mann, Jr., and F. G. Yost, The flow of liquids in surface grooves, *Langmuir, 12*, 555–565, 1996.

Shetty, S., and R. L. Cerro, Flow of a thin film over a periodic surface, *Int. J. Multiphase Flow, 19*, 1013–1027, 1993.

Sposito, G., *The Thermodynamics of Soil Solutions*, 223 pp., Oxford Univ. Press, New York, 1981.

Stephens, D. B., A perspective on diffuse natural recharge mechanisms in areas of low precipitation, *Soil Sci. Soc. Am. J., 58*, 40–48, 1994.

Taylor, J. R., *An Introduction to Error Analysis: The Study of Uncertainties in Physical Measurements*, 270 pp., Univ. Sci. Books, Mill Valley, Calif., 1982.

Taylor, S. A., and G. L. Ashcroft, *Physical Edaphology: The Physics of Irrigated and Nonirrigated Soils*, 533 pp., W. H. Freeman, San Francisco, Calif., 1972.

Tokunaga, T. K., A tensiometer for measuring hydraulic potentials on surfaces of porous rock, *Water Resour. Res.*, this issue.

Toledo, P. G., R. A. Novy, H. T. Davis, and L. E. Scriven, Hydraulic conductivity of porous media at low water content, *Soil Sci. Soc. Am. J., 54*, 673–679, 1990.

Wan, J., T. K. Tokunaga, C. F. Tsang, and G. S. Bodvarsson, Improved glass micromodel methods for studies of flow and transport in fractured porous media, *Water Resour. Res., 32*, 1955–1964, 1996.

Wang, J. S. Y., and T. N. Narasimhan, Hydrologic mechanisms governing fluid flow in a partially saturated, fractured, porous medium, *Water Resour. Res., 21*, 1861–1874, 1985.

Wang, J. S. Y., and T. N. Narasimhan, Unsaturated flow in fractured porous media, in *Flow and Contaminant Transport in Fractured Rock*, edited by J. Bear, C. F. Tsang, and G. de Marsily, pp. 325–394, Academic, San Diego, Calif., 1993.

Wang, J. S. Y., N. G. W. Cook, H. A. Wollenberg, C. L. Carnahan, I. Javandel, and C. F. Tsang, Geohydrological data and models of Rainier Mesa and their implications to Yucca Mountain, High Level Radioactive Waste Management, paper presented at 4th Annual International Conference, Am. Nucl. Soc., Las Vegas, Nev., 1993.

White, R. E., The influence of macropores on he transport of dissolved and suspended matter through soil, *Adv. Soil Sci., 3*, 95–120, 1985.

Zhao, L., and R. L. Cerro, Experimental characterization of viscous film flows over complex surfaces, *Int. J. Multiphase Flow., 18*, 495–516, 1992.

Zimmerman, R. W., and G. S. Bodvarsson, Hydraulic conductivity of rock fractures, *Transp. Porous Media, 23*, 1–30, 1996.

T. K. Tokunaga and J. Wan, Lawrence Berkeley National Laboratory, 1 Cyclotron Rd., MS 90-1116, Berkeley, CA 94720. (e-mail: tktokunaga@lbl.gov)

(Received September 13, 1996; revised December 23, 1996; accepted February 14, 1997.)